Apolipoprotein D overexpression alters hepatic prostaglandin and omega fatty acid metabolism during the development of a non-inflammatory hepatic steatosis

Frederik Desmarais, Karl-F. Bergeron, Eric Rassart, Catherine Mounier

Molecular Metabolism of Lipids Laboratory, BioMed Research Center, Biological Sciences Department, University of Quebec in Montreal (UQAM)

Abstract

Apolipoprotein D (ApoD) is a secreted lipocalin associated with neuroprotection and lipid metabolism. Overexpression of ApoD in mouse neural tissue induces the development of a non-inflammatory hepatic steatosis in 12-month-old transgenic animals. Previous data indicates that accumulation of arachidonic acid, ApoD's preferential ligand, and overactivation of PPARγ are likely the driving forces in the development of the pathology. However, the lack of inflammation under those conditions is surprising. Hence, we further investigated the apparent repression of inflammation during hepatic steatosis development in aging transgenic animals. The earliest modulation of lipid metabolism and inflammation occurred at 6 months with a transient overexpression of L-PGDS and concomitant overproduction of 15d-PGJ_2, a PPARγ agonist. Hepatic lipid accumulation was detectable as soon as 9 months. Inflammatory polarization balance varied in time, with a robust anti-inflammatory profile at 6 months coinciding with 15d-PGJ_2 overproduction. Omega-3 and omega-6 fatty acids were preferentially stored in the liver of 12-month-old transgenic mice and resulted in a higher omega-3/omega-6 ratio compared to wild type mice of the same age. Thus, inflammation seems to be controlled by several mechanisms in the liver of transgenic mice: first by an increase in 15d-PGJ_2 production and later by a beneficial omega-3/omega-6 ratio. PPARγ seems to play important roles in these processes. The accumulation of several omega fatty acids species in the transgenic mouse liver suggests that ApoD might bind to a broader range of fatty acids than previously thought.

Keywords

Apolipoprotein D, hepatic steatosis, prostaglandin 15d-PGJ_2, omega-6 fatty acid, omega-3 fatty acid, peroxisome proliferator-activated receptor γ

1. INTRODUCTION

Apolipoprotein D (ApoD) is a 25 to 30 kDa glycosylated protein member of the lipocalin superfamily [1-4]. Its known biological functions are associated to its capacity to bind several small hydrophobic molecules [5]. In mice, ApoD expression is limited to the central nervous system (CNS). In humans however, ApoD is expressed in the CNS, adrenal glands, kidneys, pancreas, placenta, spleen, lungs, ovaries and testes [6]. Because ApoD is massively overexpressed (up to 500-fold) during neurodegenerative stress [7, 8], it has mainly been studied in a neural context. Some of ApoD's functions are mediated by its capacity to bind arachidonic acid (ARA) [9], a polyunsaturated omega-6 fatty acid with the highest affinity among known ApoD ligands [10]. In recent years, roles for ApoD outside the CNS have begun to emerge.

Overexpression of human ApoD (hApoD) in transgenic mice under the neuron-specific *THY1* promoter triggers a hepatic steatosis without hepatitis at 12 months of age [11]. Transgenic hApoD mouse livers are characterized by an overactivation of the peroxisome proliferator-activated receptor gamma (PPARγ) transcription factor, higher expression of the PPARγ target cluster of differentiation 36 (CD36) and higher fatty acid uptake. Lipogenesis, however, is largely unaffected [12]. In general, hepatic lipid accumulation is thought to lead to inflammation which, in turn, exacerbates lipid accumulation (two-hit hypothesis) [13]. This is not the case in the livers of 12 month-old hApoD animals [11]. No data has yet been collected from younger hApoD mice. The absence of hepatic inflammation in the transgenic mouse is particularly intriguing as hApoD livers are rich in ARA [12], a precursor for series 2 prostaglandins (PGE_2, PGI_2, PGD_2, etc.) and series 4 leukotrienes (LTA_4, LTB_4, LTC_4, etc.) [14], molecules intimately associated with inflammation. We therefore set out to pinpoint the processes taking place in the livers of aging hApoD mice, specifically lipid accumulation, inflammation modulation and prostaglandin production.

2. MATERIALS AND METHODS

2.1 Animals

Experimental procedures were approved by the Animal Care and Use Committee (CIPA) of the University of Quebec in Montreal (UQAM). Animals were housed at 24 ± 1°C in a 12h light / 12h dark cycle and fed a standard rodent chow (Charles River, #5075) *ad libitum* with free access to

water. Tg(THY1-APOD1)1Era (hApoD) mice, expressing a human *APOD* cDNA under a 3.5 kb fragment of the human *THY1* promoter/enhancer region, were continuously backcrossed with C57BL/6 mice to maintain a heterozygous transgenic population. Experiments were carried out on males aged 3, 6, 9 and 12 months. Mice were first anaesthetised by inhalation of 5% isoflurane and then euthanized by CO_2 inhalation. Blood was promptly collected (~500 µL). Livers were collected, washed in PBS, flash frozen in liquid nitrogen and stored at -80°C. Mouse genotyping was performed as previously described [11]. DNA concentration was assessed using a NanoDrop 2000 (Thermo Scientific, ND2000). PCR was performed using Taq DNA polymerase (Invitrogen, 18038-042) with 60 ng of DNA and 10mM primers (hApoD forward: ACA AGC ATT TCA TCT TGG GAA GT and reverse: CAT CAG CTC TCA ACT CCT GGT; *Actb* control forward: GAT GTC ACG CAC GAT TTC CC and reverse: CCC AGC ACA CTG AAC TTA GC). PCR products were separated on 1% agarose gel and visualised after incubation in ethidium bromide 0.5 µg/mL.

2.2 RNA extraction and quantitative PCR

Total RNA was extracted from liver samples using TRIzol Reagent (Life Technologies, 15596-018) according to the manufacturer's protocol. Four µg of total RNA was then reverse-transcribed to cDNA using SuperScript II reverse transcriptase (Invitrogen, 18064-022). Quantitative PCR (qPCR) was performed in a LightCycler 480 thermocycler (Roche, 05015278001). A preliminary qPCR array was performed using a predesigned prostaglandin 2 series biosynthesis and metabolism panel (BioRad, 100-29146) as well as a custom inflammatory balance panel (BioRad). Standard qPCR were performed with Luna Universal qPCR Master Mix and specific primers (**Table A1**) using *Hprt* as a reference gene. To help represent the inflammatory balance in hepatic tissue, a polarization index (equation below) was calculated taking into consideration M0, M1 and M2 marker expression. High values indicate a bias towards inflammation. This index was calculated for each liver.

$$Polarisation\ index = \frac{(Cd68 + Adgre1) + (Tnf\alpha + Il1\beta + Il6) - (Tgf1b + Cd163)}{7}$$

2.3 Immunoblotting

For whole cell extractions, liver samples were homogenized in lysis buffer (50mM Tris-HCl pH 7.4, sucrose 250mM, 100mM NaF, 10mM sodium pyrophosphate, 1mM EDTA, 1mM DTT, 1mM sodium vanadate, 1mM PMSF). Lysates were then incubated 30 min at 4°C, cleared by centrifugation (10,000 g, 15 min). The lipid layer was discarded and protein concentration was assessed by Bradford assay [15]. For nuclear enrichment, liver samples were first homogenised

in lysis buffer (10mM HEPES, 1.5mM $MgCl_2$, 10mM KCl, 0,5mM DTT and 0.05% NP-40, pH 7.9). The nuclear fraction was precipitated by centrifugation (1,500 g, 10 min), then resuspended in a second buffer (5mM HEPES, 1.5mM $MgCl_2$, 0.2mM EDTA, 0.5 mM DTT and 26% glycerol (v/v), pH 7.9) and homogenised in a Dounce tissue grinder (Wheaton, 357421). Remaining cell debris were removed by centrifugation (24,000 g, 20 min). Protein concentration was assessed by Bradford assay [15]. Proteins (20 µg) were separated on SDS-PAGE and transferred on PVDF membrane. Blocking was performed using 5% milk, 1h at room temperature. Membranes were then incubated with primary antibodies overnight at $4^{o}C$. Dilutions of the primary antibodies were of 1:50,000 for cyclophilin B (Abcam, ab16045), 1:1000 for PPARγ (Abcam, ab45036), SREBP-1 (Santa Cruz, sc13551) FASN (Abcam, ab22759) and NF-κB p50 (Santa Cruz, sc7178). Primary antibodies were detected using goat anti-rabbit HRP conjugated IgG antibodies (Cell Signaling Tech., 7074S) at 1:1000 and visualized by using chemiluminescent HRP substrate (Millipore, WBKLS0500). Amidoblack staining was used as a loading control. Briefly, membranes were stained for 20 min in amidoblack solution (0.1% amidoblack, 40% v/v methanol and 10% v/v acetic acid) and washed 10 min twice in decolouration solution (40% v/v methanol and 10% v/v acetic acid). Bands were quantified by densitometry using Image J software.

2.4 Enzyme-linked immunosorbent assays

Liver extracts were prepared by homogenizing tissues in cold lysis buffer (50mM Tris-HCl pH 7.3, 150 mM NaCl, 5 mM EDTA, 0.2% Triton X-100, 2 mM sodium orthovanadate and 10% cOmplete protease inhibitor). Lysates were then incubated 30 min at 4°C and cleared by centrifugation (10000 g, 15 min). The concentration of PGE_2 and 15d-PGJ_2 were then measured using specific ELISA kits (Enzo Life Sciences, PGE_2: ADI-900-001, 15d-PGJ_2: ADI-900-023) according to the manufacturer's protocol. For PGD_2, liver extracts where homogenised in cold PBS. PGD_2 was then measured using the prostaglandin D_2-MOX Express ELISA Kit (Cayman chemical, 500151).

2.5 Histology

Frozen liver sections were prepared by first freezing samples in NEG-50 (Thermo Scientific, 6502) and cutting 4 µm slices with a cryostat (Leica, CM1950). Sections were then fixed in PBS containing 4% paraformaldehyde. To visualise neutral lipids, sections were stained with 0.5% Oil Red O in isopropanol and counterstained with 0.5% hematoxylin. Lipid accumulation was quantified by determining the number of red pixels (Oil Red O-stained lipids) relative to blue pixels (hematoxylin-stained nuclei) using the color threshold function of Image J software.

Paraffin sections were also prepared by fixing liver samples in Bouin's solution overnight at room temperature before paraffin embedding. Microtome 8 µm sections were then stained with Masson's Trichrome. Histology scoring for macrovesicular and microvesicular steatosis, in addition to inflammation foci and fibrosis was performed by an independent hepatologist following a Kleiner scoring system adapted for rodents [16, 17].

2.6 Fatty acid profiling

Fatty acid composition was measured by a modified gas chromatography-mass spectrometry (GC-MS) method, as previously described [18]. Briefly, total lipids were extracted from plasma with a mixture of methyl tert-butyl ether, methanol and water [19]. For liver, pulverized tissues (25mg) were incubated overnight at 4°C in a solution of chloroform/methanol (2:1) containing 0.004% butylated hydroxytoluene, filtered through gauze and dried under nitrogen gas. Plasma and liver fatty acids were analyzed as their fatty acid methyl derivatives (FAME) after direct transesterification with acetyl chloride/methanol [20]. Injections (2 µL for plasma and 1 µL for liver samples) were performed onto an Agilent 7890B gas chromatograph equipped with a Select FAME CP7420 capillary column (100 m; 250 µm inner diameter; 230 µm thickness) coupled with a 5977A Mass Selective Detector operated in positive chemical ionisation mode using ammonia as reagent gas. Fatty acids were identified according to their retention time and m/z, and their concentration was calculated using a mix of internal and external labelled standards added to liver and plasma samples at known concentrations. The concentration of fatty acid is reported relative to total fatty acid content (%).

2.7 Statistics

Results are presented as mean ± standard error mean unless otherwise stated. Statistical analysis was performed with GraphPad 5 software. Statistically significant differences from control values (*p-value* <0.05 or less) were determined by a one-tailed Student's t-test. A Welch's correction was applied when variances between groups were unequal (as determined by the Fisher's f-test).

3. RESULTS

3.1 Hepatic lipid accumulation is apparent at 9 months of age

We first examined the livers of wild type (WT) and transgenic hApoD mice at every trimester leading up to 12 months of age. Neutral lipid accumulation (**Fig.1A)** and macrovesicular steatosis (**Fig.1B**) were already apparent in transgenic livers at 9 months and increased during the next trimester. Several transgenic hepatic samples reached score 3 macrovesicular steatosis at 12 months, while WT animals of the same age only exhibited early signs of age-related steatosis (grade 1; **Fig.1B**). No difference in microvesicular steatosis or fibrosis scores were observed between WT and hApoD livers (data not shown).

3.2 Lipid uptake increases at 6 months

Next, we examined the effect of hApoD overexpression on hepatic lipid synthesis by evaluating activation of the transcription factor SREBP-1 and expression of its target FASN. The maturation by cleavage of SREBP-1, the master regulator of hepatic lipogenesis, was not significantly modulated in hApoD mice livers compared to WT controls, except for a slight activation at 12 months (**Fig.2A**). FASN levels were also fairly stable, except for a slight increase at 3 months (**Fig.2B**). We also investigated hepatic lipid uptake via the evaluation of PPARγ and *Cd36* levels. PPARγ protein levels were increased in nucleus-enriched fractions of hApoD livers starting at 6 months (**Figs.2C and A1**). This was reflected by an overexpression of its transcription target *Cd36* beginning at the same trimester (**Fig.2D**). These results further establish lipid uptake via PPARγ activation as the mechanism by which fatty acids accumulate in the livers of hApoD mice [12].

3.3 Anti-inflammatory profile at 6 months

Despite the pronounced hepatic steatosis established by 12 months of age, hApoD mice do not develop the steatohepatitis that is typically associated with it [21]. To better understand this unexpected phenomenon, we measured the expression of macrophage polarization biomarkers within liver tissue at every trimester. There was a trend toward M1 pro-inflammatory polarization at 3 and 9 months, a trend towards M2 anti-inflammatory polarization at 6 months and a mostly neutral profile at 12 months. These trends were particularly pronounced at 6 and 9 months, as revealed by their respective polarization indexes (**Fig.3A**). While transgenic livers appeared to experience episodes of pro-inflammatory polarization, these did not result in increased macrophage recruitment. In fact, the severity of inflammatory foci was never elevated relative to WT controls (**Fig.3B**). Interestingly, no inflammatory foci could be observed in 6-month-old M2-polarized hApoD livers. This correlates with a strong reduction of the nuclear recruitment of NF-κB (p50) at 6 months and a moderate reduction at 12 months (**Fig.3C).**

3.4 Overproduction of prostaglandin D_2 and 15d-PGJ_2

We next examined whether ARA accumulation in aging hApoD transgenic livers [12] translated into an overproduction of prostaglandins. A preliminary qPCR screen (**Fig.A1**), guided our investigation towards the production of two specific prostaglandins: PGE_2 and PGD_2. We also chose to investigate 15d-PGJ_2, a non enzymatic derivative of PGD_2, because of its potent anti-inflammatory and pro-lipogenic properties [22-24]. We observed an increase in the hepatic expression of COX-2 (*Ptgs2* gene) and L-PGDS (*Ptgds* gene) at 6 months (**Fig.4A**), two enzymes participating in the conversion of ARA into PGD_2. Accordingly, we observed a significant increase of the anti-inflammatory prostaglandin 15d-PGJ_2 at 6 months (**Fig.4B**). We also observed increased PGD_2 levels at 12 months. The pro-inflammatory prostaglandin PGE_2 remained unmodulated at all trimesters, a result consistent with our previous published data on 12-month-old hApoD livers [12].

3.5 Omega fatty acid accumulation during aging

To better understand the steatosis process in hApoD livers, we measured a large panel of fatty acids in aging hApoD and WT livers, including several saturated, mono-unsaturated and omega (ω)-3/6/9 fatty acids (**Figs.A2 and A3**). In WT livers, the proportion of [saturated + mono-unsaturated] fatty acids among the total pool of fatty acids increased progressively with age (**Fig.5A**) while the proportion of [ω-3 + ω-6] fatty acids diminished (**Fig.5B**). This was not observed in transgenic fatty livers, as these fatty acid proportions were similar at all ages. In addition, every ω-3 and ω-6 fatty acid quantified in our experiment was elevated in 12-month-old hApoD fatty livers compared to WT controls (**Fig.5C**). Interestingly, in terms of inflammation potential, the ω-3/ω-6 fatty acid ratio in hApoD livers was lower at 3 months and higher at 12 months (**Fig.5D**). As ApoD is a secreted protein [1, 4, 25, 26], we hypothesized that its overexpression might modify circulating lipid levels. Indeed, compared to WT mice, the plasmatic ω-6 fatty acids ARA and dihomo-γ-linoleic acid (DGLA) were lowered while the ω-3 docosapentaenoic acid (DPA) was slightly increased in 12-month-old hApoD mice (**Fig.5E**).

4. DISCUSSION

Our previous study has implicated an increase in lipid uptake associated with PPARγ activation in the development of hepatic steatosis in hApoD mice [12]. Fatty acid accumulation is typically associated with hepatic inflammation (steatohepatitis) [27]. The goal of this new study was to

provide a better understanding of the intriguing absence of inflammation in the hApoD fatty liver. A model explaining our findings is presented in **Figure 6**.

The earliest event we uncovered was the production of 15d-PGJ_2 in 6-month-old hApoD livers (**Fig.4B**), a full trimester before hepatic lipid accumulation was detectable by microscopy analysis. This prostaglandin being a strong PPARγ agonist [28], 15d-PGJ_2 could be directly responsible for PPARγ activation in hApoD livers. Despite the fact that 15d-PGJ_2 was only transiently overproduced, PPARγ remained activated in the following trimesters. The *Cd36* gene is transcriptionally activated by PPARγ [29]. Consequently, increased expression of CD36 which mediates the cellular uptake of long chain fatty acids (LCFA) and poly-unsaturated fatty acids (PUFA) [30, 31] leads to increased LCFA and PUFA concentration that can in turn, activate PPARγ [32]. Therefore, increased CD36 expression could result in a positive feedback loop maintaining PPARγ activation after 6 months.

The IKK/NF-κB pathway plays an important role in liver inflammation [33]. Prostaglandin 15d-PGJ_2 can inhibit NF-κB signaling through PPARγ-dependent and -independent mechanisms. Agonist-bound PPARγ reduces NF-κB transcriptional activity in a dose-dependent manner [34]. Moreover, 15d-PGJ_2 can disrupt NF-κB signaling through covalent modification of a cysteine residue (Michael addition reaction) in IKK and in the DNA binding domain of NF-κB itself [35, 36]. The overproduction of 15d-PGJ_2 was indeed concomitant to a strong inhibition of NF-κB (p50) nuclear recruitment at 6 months (**Fig.3C**). By inhibiting NF-kB signaling, 15d-PGJ_2 production could contribute to the strong anti-inflammatory profile observed in hApoD livers at 6 months, where the severity of inflammation foci tended to be even lower than in WT livers (**Fig.3B**). In fact, injection of 15d-PGJ_2 was previously shown to inhibit hepatic inflammation *in vivo* [37, 38]. PGD_2 is an unstable compound and the molecular precursor of 15d-PGJ_2 and other J_2 prostaglandins through non-enzymatic reactions. We found that PGD_2 levels seemed to be higher at 6 months and were significantly higher at 12 months in hApoD mice livers. Like 15d-PGJ_2, PGD_2 plays anti-inflammatory functions in the liver [39]. Thus, PGD_2 could help promote an anti-inflammatory environment in 12-month-old hApoD mice livers.

Another mitigating factor towards the advent of steatohepatitis is the fact that a great proportion of fatty acids identified in the hApoD fatty liver were ω-6 and ω-3 PUFA. Lipotoxicity is typically associated with accumulation of saturated fatty acids such as palmitate [40] and mono-unsaturated fatty acids like oleate [41]. Relative to WT controls, transgenic fatty livers accumulate a smaller proportion of saturated and mono-unsaturated LCFA in favour of ω-6 and ω-3 fatty acids (**Fig.5A&B**). In addition, as ω-3 fatty acids possess anti-inflammatory properties

[42, 43]. The higher ω-3/ω-6 ratio presumably contributes to inflammation suppression in hApoD livers (**Fig.5C**).

The circulating lipid transporter ApoD could directly contribute to fatty acid accumulation in transgenic livers. ApoD has been shown to be internalized in several cell types [44-46], a process that could participate in intracellular lipid accumulation. ARA, the ApoD ligand with the highest known affinity [1, 47], is accordingly depleted in plasma and accumulates in hApoD liver tissue. However, transgenic livers accumulated not only ARA but also all the other ω-3 and ω-6 fatty acids measured in our study (**Fig.5D**). This suggests that ApoD could bind many different ω fatty acids and transport them to the liver. In accordance with this concept, DGLA (C20:3n6), which is structurally similar to ARA (C20:4n6), was also depleted from hApoD plasma (**Fig.5E**).

The production of 15d-PGJ_2 in 6-month-old hApoD livers was presumably due to the concomitant expression of COX-2 and L-PGDS (**Fig.4A**). However, the events responsible for the increase in COX-2 and L-PGDS expression are still not known. One possibility is that a sub-population of liver tissue cells are first affected by circulating ApoD in transgenic mice. Endothelial cells would be the first liver cells to come in contact with circulating lipid-charged ApoD. Hepatic endothelial cells express L-PGDS (*Ptgds* gene) [48-52]. Therefore, 15d-PGJ_2 overproduction could be the result of ARA transformation within endothelial cells. Hepatocytes also express L-PGDS [53, 54], but despite their prevalence in liver tissue (roughly 92.5% of liver mass), they only produce a small proportion of total hepatic eicosanoids (12%) compared to endothelial and Kupffer cells (23% and 65%, respectively) [55]. While Kupffer cells are known to produce 15d-PGJ_2, their ability to do so is not dependent upon the *Ptgds* gene but upon *Hpgds* [56, 57] which was not modulated in hApoD livers. Together, these considerations highlight the possibility that hepatic endothelial cells are implicated in the early inflammatory and metabolic processes taking place in the hApoD mouse liver (**Fig.7**).

The expression of COX-2 and L-PGDS is dependent on several transcription factors, one of which is NF-κB. However, the mRNA overexpression observed in hApoD livers at 6 months (**Fig.4A**) cannot be dependent on NF-kB since it is underactivated (**Fig.3C**). Other transcription factors such as AP-1, AP-2 and CREB also regulate COX-2 [58] and L-PGDS [59] expression. Exogenous ARA can induce AP-1 transcriptional activity without involving the NF-κB pathway [60]. Additionally, 15d-PGJ_2 can induce COX-2 overexpression by activation of AKT and subsequently AP-1 [61]. Following the model proposed in **Figure 7**, ARA accumulation in endothelial cells could activate COX-2 and L-PGDS overexpression through activation of transcription factors (such as AP-1), resulting in PGD_2 and 15d-PGJ_2 overproduction.

In conclusion, we have uncovered processes through which ApoD can modulate hepatic prostaglandin production and omega fatty acid accumulation, resulting in a non-inflammatory hepatic steatosis in transgenic hApoD mice.

Author Contributions

FD performed the experiments. FD and KFB wrote the manuscript. CM and ER edited the manuscript and supervised the study.

Disclosure Statement

The authors declare that they have no competing interests.

Acknowledgements

We are grateful to Dr Natasha Patey (hepatologist at Sainte-Justine Hospital, Montreal) for the independent grading of steatosis and inflammation on histology slides of hepatic tissue.

5. REFERENCES

1. Rassart, E., et al., *Apolipoprotein D.* Biochim Biophys Acta, 2000. **1482**(1-2): p. 185-98.
2. Li, H., et al., *Cerebral Apolipoprotein-D Is Hypoglycosylated Compared to Peripheral Tissues and Is Variably Expressed in Mouse and Human Brain Regions.* PLoS One, 2016. **11**(2): p. e0148238.
3. Kielkopf, C.S., et al., *Identification of a novel tetrameric structure for human apolipoprotein-D.* J Struct Biol, 2018.
4. Balbín, M., et al., *Apolipoprotein D is the major protein component in cyst fluid from women with human gross cystic disease.* Biochem J, 1990. **271**: p. 803-807.
5. Muffat, J. and D.W. Walker, *Apolipoprotein D: an overview of its role in aging and age-related diseases.* Cell Cycle, 2010. **9**(2): p. 269-73.
6. Drayna, D., et al., *Cloning and expression of human Apolipoprotein D cDNA.* Journal of Biological chemistry, 1986. **261**(december 15): p. 16535-16539.
7. Boyles, J.K., L.M. Notterpek, and L.J. Anderson, *Accumulation of apolipoproteins in the regenerating and remyelinating mammalian peripheral nerve. Identification of apolipoprotein D, apolipoprotein A-IV, apolipoprotein E, and apolipoprotein A-I.* J Biol Chem, 1990. **265**(29): p. 17805-15.
8. Boyles, J.K., et al., *Identification, characterization, and tissue distribution of apolipoprotein D in the rat.* J Lipid Res, 1990. **31**(12): p. 2243-56.
9. Thomas, E.A., R.C. George, and J.G. Sutcliffe, *Apolipoprotein D modulates arachidonic acid signaling in cultured cells: implications for psychiatric disorders.* Prostaglandins, Leukotrienes and Essential Fatty Acids, 2003. **69**(6): p. 421-427.
10. Morais Cabral, J.H., et al., *Arachidonic acid binds to apolipoprotein D: implications for the protein's function.* FEBS Letters, 1995. **366**(1): p. 53-56.
11. Do Carmo, S., et al., *Human apolipoprotein D overexpression in transgenic mice induces insulin resistance and alters lipid metabolism.* Am J Physiol Endocrinol Metab, 2009. **296**(4): p. E802-11.
12. Labrie, M., et al., *Apolipoprotein D Transgenic Mice Develop Hepatic Steatosis through Activation of PPARgamma and Fatty Acid Uptake.* PLoS One, 2015. **10**(6): p. e0130230.
13. Dowman, J.K., J.W. Tomlinson, and P.N. Newsome, *Pathogenesis of non-alcoholic fatty liver disease.* QJM, 2010. **103**(2): p. 71-83.
14. Funk, C.D., *Prostaglandins and leukotrienes: advances in eicosanoid biology.* Science, 2001. **294**(5548): p. 1871-5.
15. Bradford, M.M., *A rapid and sensitive method for the quantitation of microgram quantities of protein utilizing the principle of protein-dye binding.* Analytical Biochemistry, 1976. **72**(1-2): p. 248-254.
16. Kleiner, D.E., et al., *Design and validation of a histological scoring system for nonalcoholic fatty liver disease.* Hepatology, 2005. **41**(6): p. 1313-21.
17. Liang, W., et al., *Establishment of a general NAFLD scoring system for rodent models and comparison to human liver pathology.* PLoS One, 2014. **9**(12): p. e115922.
18. Gelinas, R., et al., *Prolonged QT interval and lipid alterations beyond beta-oxidation in very long-chain acyl-CoA dehydrogenase null mouse hearts.* Am J Physiol Heart Circ Physiol, 2011. **301**(3): p. H813-23.
19. Matyash, V., et al., *Lipid extraction by methyl-tert-butyl ether for high-throughput lipidomics.* J Lipid Res, 2008. **49**(5): p. 1137-46.
20. Lepage, G. and C.C. Roy, *Direct transesterification of all classes of lipids in a one-step reaction.* J Lipid Res, 1986. **27**(1): p. 114-20.
21. Do Carmo, S., et al., *Human apolipoprotein D overexpression in transgenic mice induces insulin resistance and alters lipid metabolism.* Am J Physiol Endocrinol Metab., 2009. **296**(4): p. E802-11. doi: 10.1152/ajpendo.90725.2008. Epub 2009 Jan 27.

22. Bell-Parikh, L.C., et al., *Biosynthesis of 15-deoxy-Δ12,14-PGJ2 and the ligation of PPARγ.* Journal of Clinical Investigation, 2003. **112**(6): p. 945-955.
23. Hashimoto, K., et al., *The PPARγ Ligand, 15d-PGJ2, Attenuates the Severity of Cerulein-Induced Acute Pancreatitis.* Pancreas, 2003. **27**(1): p. 58-66.
24. Scher, J.U. and M.H. Pillinger, *15d-PGJ2: the anti-inflammatory prostaglandin?* Clin Immunol, 2005. **114**(2): p. 100-9.
25. di Masi, A., et al., *Human plasma lipocalins and serum albumin: Plasma alternative carriers?* J Control Release, 2016. **228**: p. 191-205.
26. Ong, W.Y., et al., *Differential expression of apolipoprotein D and apolipoprotein E in the kainic acid-lesioned rat hippocampus.* Neuroscience, 1997. **79**(2): p. 359-367.
27. Suzuki, A. and A.M. Diehl, *Nonalcoholic Steatohepatitis.* Annu Rev Med, 2017. **68**: p. 85-98.
28. Kliewer, S.A., et al., *Fatty acids and eicosanoids regulate gene expression through direct interactions with peroxisome proliferator-activated receptors α and γ.* PNAS, 1997. **94**(9): p. 4318-4323.
29. Wheeler, M.C. and N. Gekakis, *Hsp90 modulates PPARgamma activity in a mouse model of nonalcoholic fatty liver disease.* J Lipid Res, 2014. **55**(8): p. 1702-10.
30. Baillie, A.G.S., C.T. Coburn, and N.A. Abumrad, *Reversible Binding of Long-chain Fatty Acids to Purified FAT, the Adipose CD36 Homolog.* Journal of Membrane Biology, 1996. **153**(1): p. 75-81.
31. Pepino, M.Y., et al., *Structure-function of CD36 and importance of fatty acid signal transduction in fat metabolism.* Annu Rev Nutr, 2014. **34**: p. 281-303.
32. Grygiel-Gorniak, B., *Peroxisome proliferator-activated receptors and their ligands: nutritional and clinical implications--a review.* Nutr J, 2014. **13**: p. 17.
33. Farrell, G.C., et al., *NASH is an Inflammatory Disorder: Pathogenic, Prognostic and Therapeutic Implications.* Gut Liver, 2012. **6**(2): p. 149-71.
34. Remels, A.H., et al., *PPARgamma inhibits NF-kappaB-dependent transcriptional activation in skeletal muscle.* Am J Physiol Endocrinol Metab, 2009. **297**(1): p. E174-83.
35. Straus, D.S., et al., *15-Deoxy-D12,14-prostaglandin J2 inhibits multiple steps in the NF-kB signaling pathway.* PNAS, 2000. **97**(9): p. 4844-4849.
36. Suh, J., et al., *15-Deoxy-Delta(12,14)-prostaglandin J2 activates PI3K-Akt signaling in human breast cancer cells through covalent modification of the tumor suppressor PTEN at cysteine 136.* Cancer Lett, 2018. **424**: p. 30-45.
37. Alves, C., et al., *Effects of 15d-PGJ(2)-loaded poly(D,L-lactide-co-glycolide) nanocapsules on inflammation.* Br J Pharmacol, 2011. **162**(3): p. 623-32.
38. Chen, K., et al., *15d-PGJ2 alleviates ConA-induced acute liver injury in mice by up-regulating HO-1 and reducing hepatic cell autophagy.* Biomed Pharmacother, 2016. **80**: p. 183-192.
39. Fujita, T. and S. Narumiya, *Roles of hepatic stellate cells in liver inflammation: a new perspective.* Inflamm Regen, 2016. **36**: p. 1.
40. Hetherington, A.M., et al., *Differential Lipotoxic Effects of Palmitate and Oleate in Activated Human Hepatic Stellate Cells and Epithelial Hepatoma Cells.* Cell Physiol Biochem, 2016. **39**(4): p. 1648-62.
41. Kitaura, Y., et al., *Enhanced oleate uptake and lipotoxicity associated with laurate.* FEBS Open Bio, 2015. **5**: p. 485-91.
42. Yates, C.M., P.C. Calder, and G. Ed Rainger, *Pharmacology and therapeutics of omega-3 polyunsaturated fatty acids in chronic inflammatory disease.* Pharmacol Ther, 2014. **141**(3): p. 272-82.
43. Jump, D.B., *The biochemistry of n-3 polyunsaturated fatty acids.* J Biol Chem, 2002. **277**(11): p. 8755-8.

44. Najyb, O., L. Brissette, and E. Rassart, *Apolipoprotein D Internalization Is a Basigin-dependent Mechanism.* J Biol Chem, 2015. **290**(26): p. 16077-87.
45. Leung, W.C., et al., *Apolipoprotein D and platelet-derived growth factor-BB synergism mediates vascular smooth muscle cell migration.* Circ Res, 2004. **95**(2): p. 179-86.
46. Do Carmo, S., L.C. Levros, Jr., and E. Rassart, *Modulation of apolipoprotein D expression and translocation under specific stress conditions.* Biochim Biophys Acta, 2007. **1773**(6): p. 954-69.
47. Dassati, S., A. Waldner, and R. Schweigreiter, *Apolipoprotein D takes center stage in the stress response of the aging and degenerative brain.* Neurobiol Aging, 2014. **35**(7): p. 1632-42.
48. Parmar, K.M., et al., *Statins exert endothelial atheroprotective effects via the KLF2 transcription factor.* J Biol Chem, 2005. **280**(29): p. 26714-9.
49. Parmar, K.M., et al., *Integration of flow-dependent endothelial phenotypes by Kruppel-like factor 2.* J Clin Invest, 2006. **116**(1): p. 49-58.
50. Roman, B.L. and K. Pekkan, *Mechanotransduction in embryonic vascular development.* Biomech Model Mechanobiol, 2012. **11**(8): p. 1149-68.
51. Taba, Y., et al., *Fluid Shear Stress Induces Lipocalin-Type Prostaglandin D2 Synthase Expression in Vascular Endothelial Cells.* Circulation Research, 2000. **86**(9): p. 967-973.
52. Miyagi, M., et al., *Activator protein-1 mediates shear stress-induced prostaglandin d synthase gene expression in vascular endothelial cells.* Arterioscler Thromb Vasc Biol, 2005. **25**(5): p. 970-5.
53. Uhlen, M., et al., *Proteomics. Tissue-based map of the human proteome.* Science, 2015. **347**(6220): p. 1260419.
54. Uhlen, M., et al., *Tissue expression of PTGDS - Staining in liver*, in *The Human Protein Atlas*. 2015, The Human Protein Atlas.
55. Kuiper, J., et al., *Identification of prostaglandin D2 as the major eicosanoid from liver endothelial and Kupffer cells.* Biochimica et Biophysica Acta (BBA) - Lipids and Lipid Metabolism, 1988. **959**(2): p. 143-152.
56. Urade, Y., et al., *The major source of endogenous prostaglandin D2 production is likely antigen-presenting cells. Localization of glutathione-requiring prostaglandin D synthetase in histiocytes, dendritic, and Kupffer cells in various rat tissues.* J Immunol, 1989. **143**(9): p. 2982-2989.
57. Zigmond, E., et al., *Infiltrating monocyte-derived macrophages and resident kupffer cells display different ontogeny and functions in acute liver injury.* J Immunol, 2014. **193**(1): p. 344-53.
58. Harper, K.A. and A.J. Tyson-Capper, *Complexity of COX-2 gene regulation.* Biochem Soc Trans, 2008. **36**(Pt 3): p. 543-5.
59. Fujimori, K., et al., *Regulation of lipocalin-type prostaglandin D synthase gene expression by Hes-1 through E-box and interleukin-1 beta via two NF-kappa B elements in rat leptomeningeal cells.* J Biol Chem, 2003. **278**(8): p. 6018-26.
60. Bécuwe, P., et al., *Arachidonic acid activates a functional AP-1 and an inactive NF-κB complex in human HepG2 hepatoma cells.* Free Radical Biology and Medicine, 2003. **35**(6): p. 636-647.
61. Kim, E.H., et al., *15-Deoxy-Delta12,14-prostaglandin J2 induces COX-2 expression through Akt-driven AP-1 activation in human breast cancer cells: a potential role of ROS.* Carcinogenesis, 2008. **29**(4): p. 688-95.

FIGURES

Figure 1

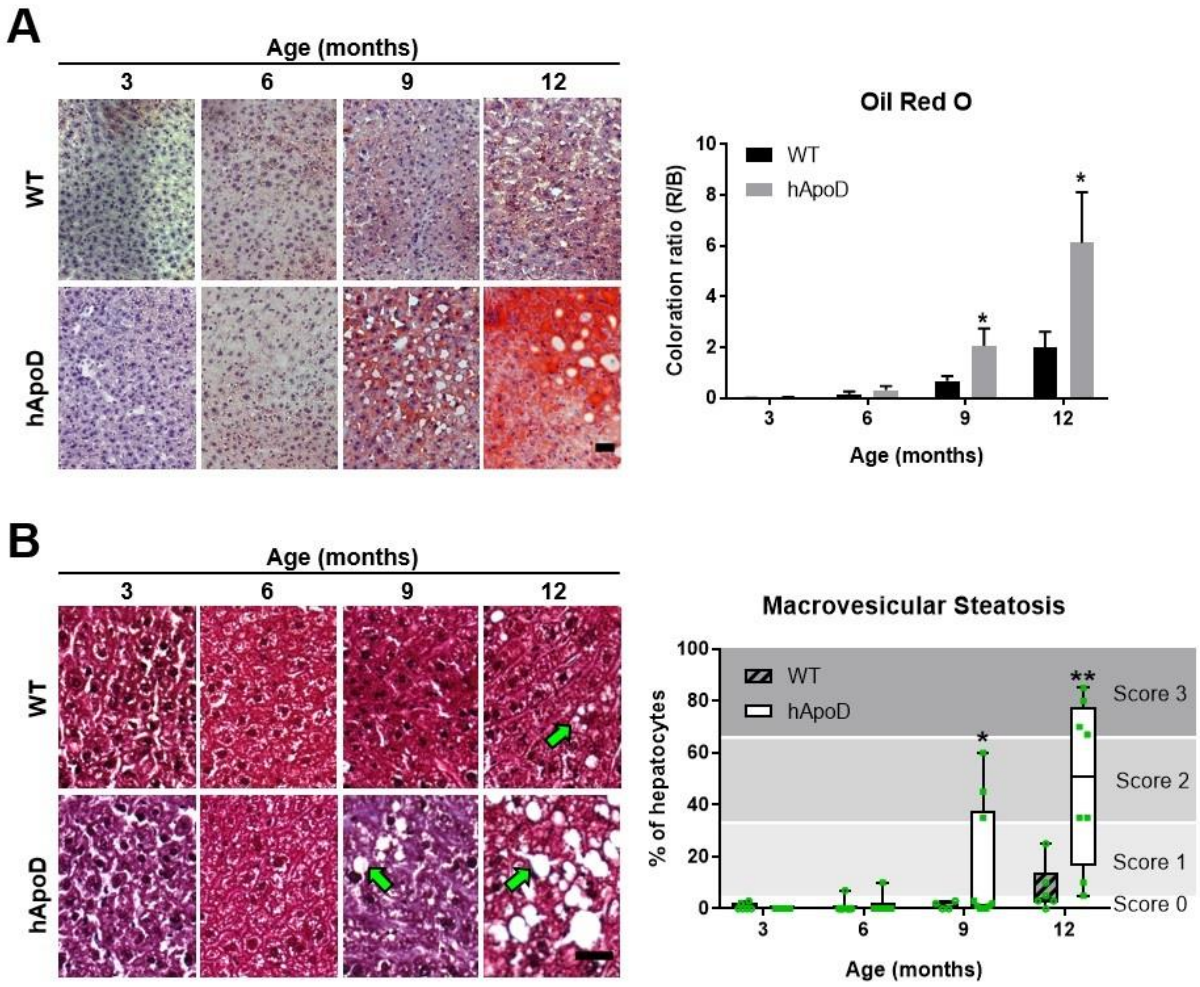

Figure 2

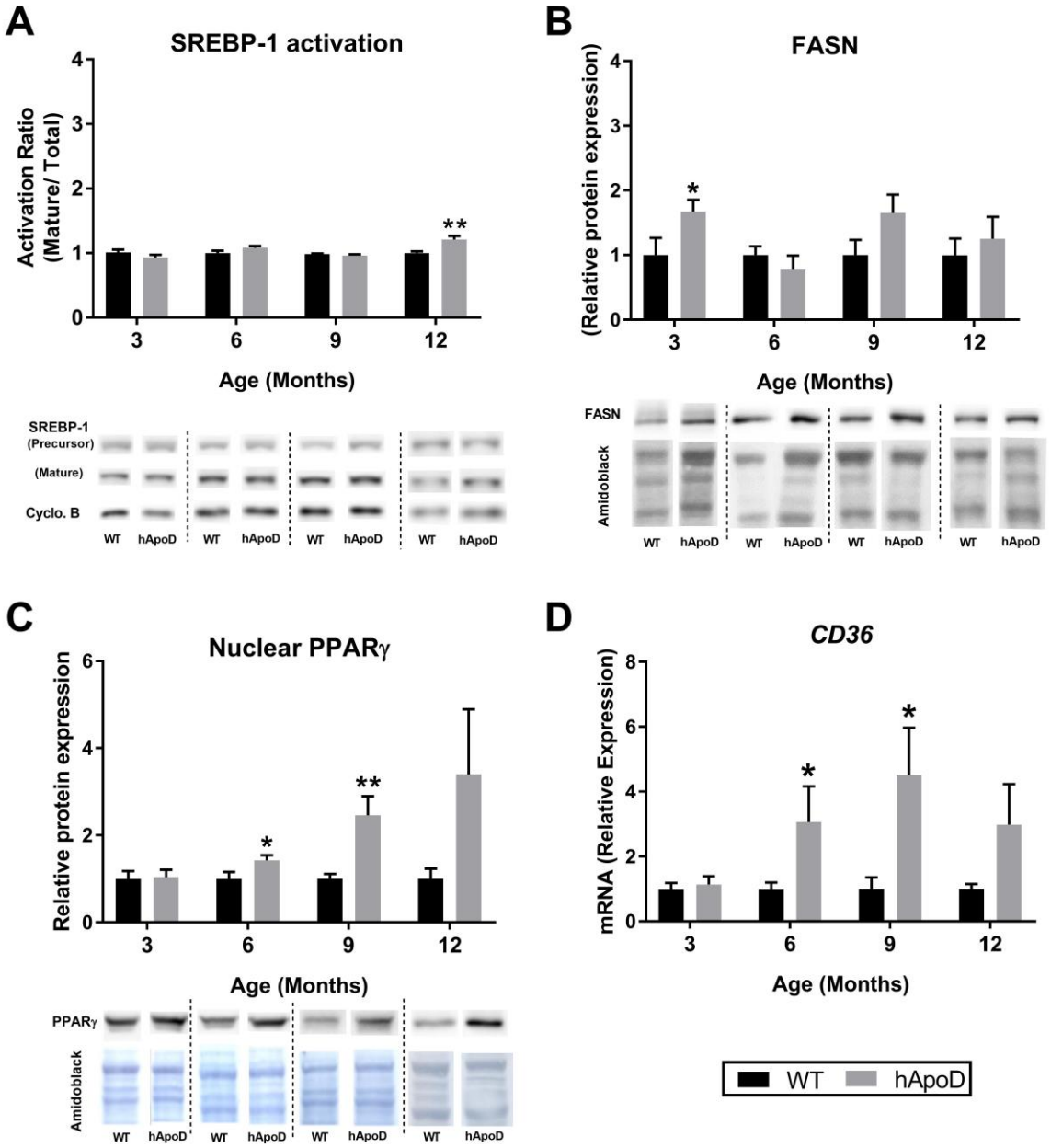
A
SREBP-1 activation
Activation Ratio (Mature/ Total)
Age (Months)
SREBP-1 (Precursor)
(Mature)
Cyclo. B
WT
hApoD
B
FASN
(Relative protein expression)
Age (Months)
FASN
Amidoblack
C
Nuclear PPARγ
Relative protein expression
Age (Months)
PPARγ
Amidoblack
D
CD36
mRNA (Relative Expression)
Age (Months)
WT
hApoD

Figure 3

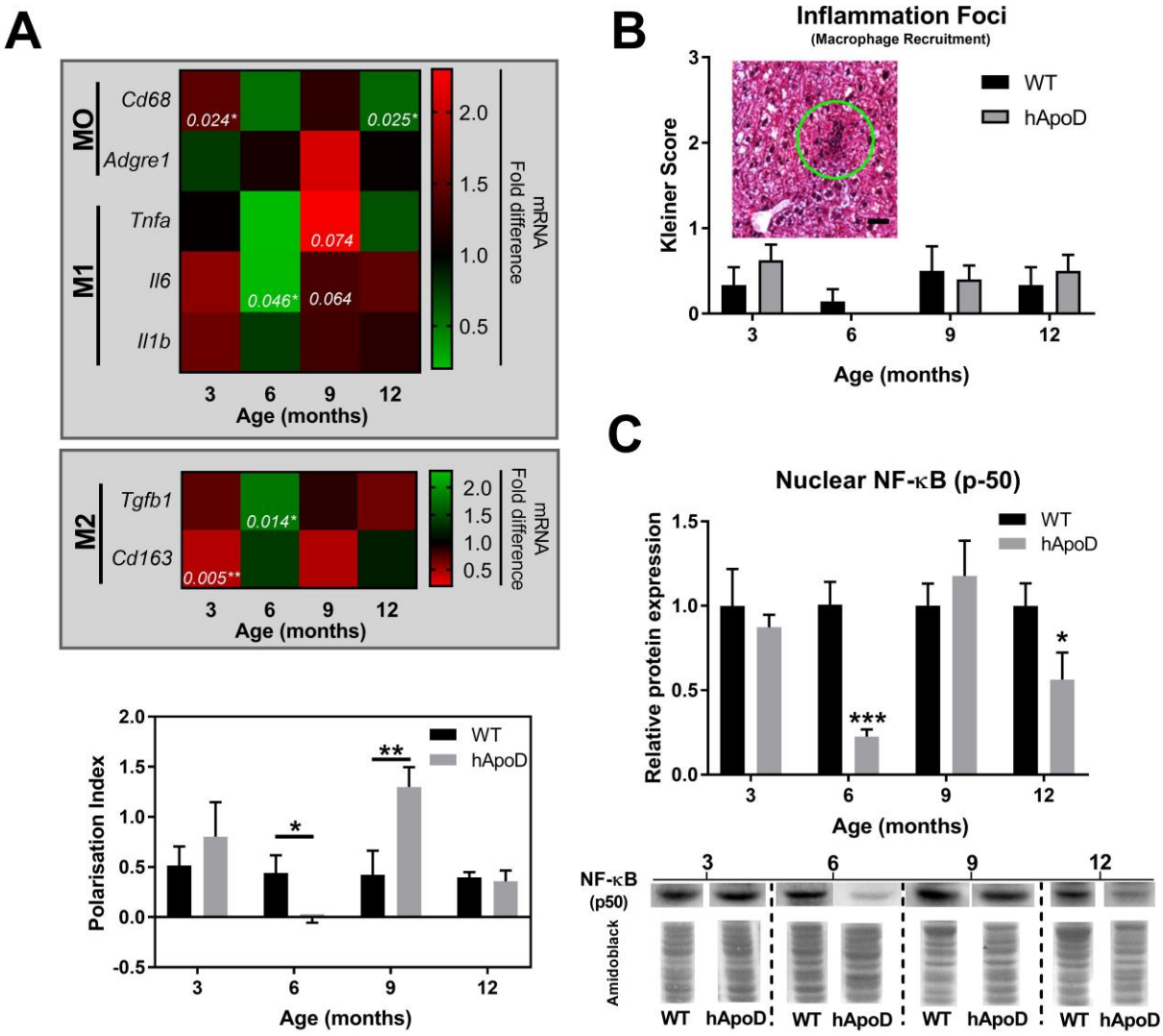
A
MO
Cd68
Adgre1
M1
Tnfa
Il6
Il1b
0.024*
0.025*
0.074
0.046*
0.064
2.0
1.5
1.0
0.5
mRNA Fold difference
3 6 9 12
Age (months)
M2
Tgfb1
Cd163
0.014*
0.005**
Polarisation Index
WT
hApoD
B
Inflammation Foci
(Macrophage Recruitment)
Kleiner Score
C
Nuclear NF-κB (p-50)
Relative protein expression
NF-κB (p50)
Amidoblack

Figure 4

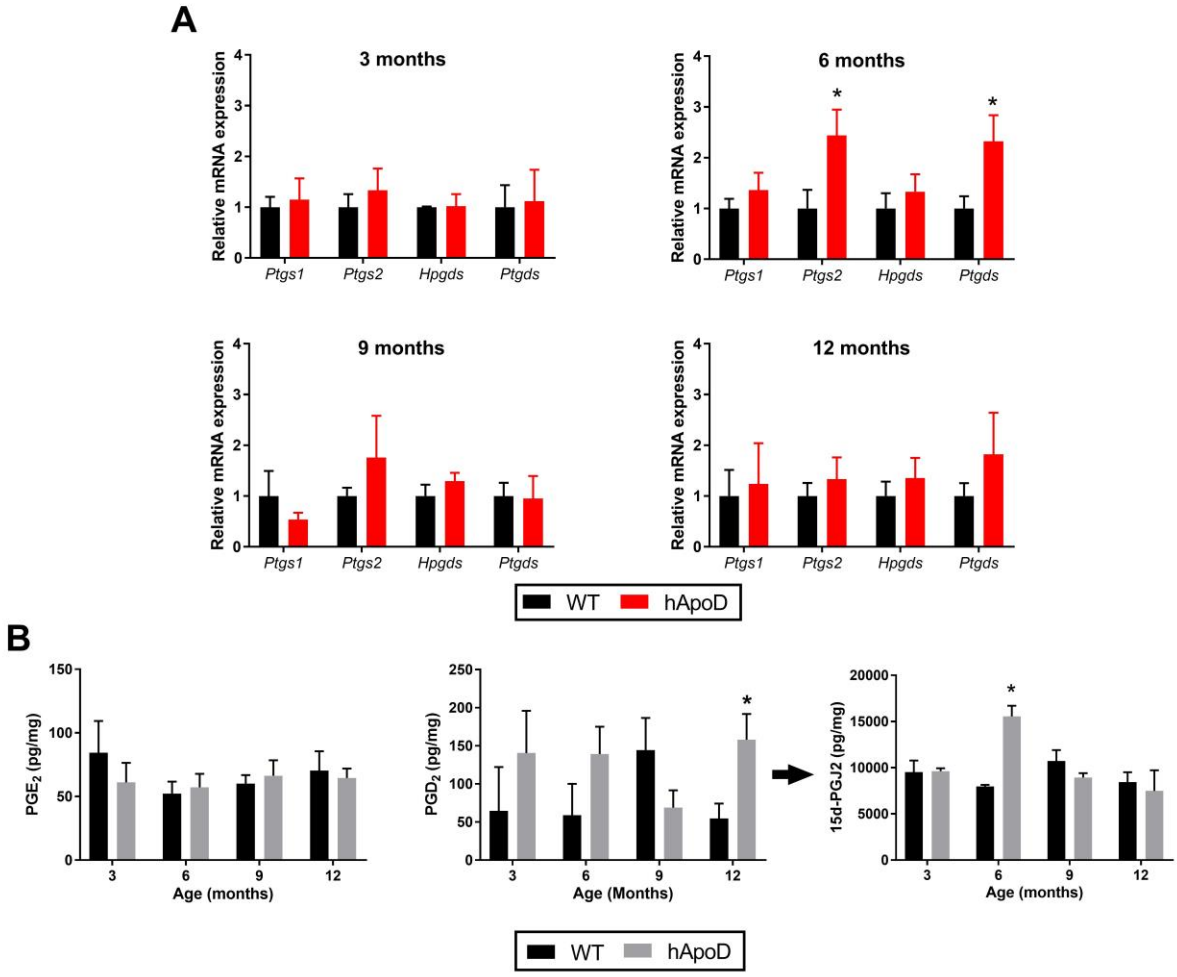
A
3 months
6 months
9 months
12 months
Relative mRNA expression
Ptgs1
Ptgs2
Hpgds
Ptgds
*
WT
hApoD
B
PGE2 (pg/mg)
PGD2 (pg/mg)
15d-PGJ2 (pg/mg)
Age (months)
Age (Months)
WT
hApoD

Figure 5

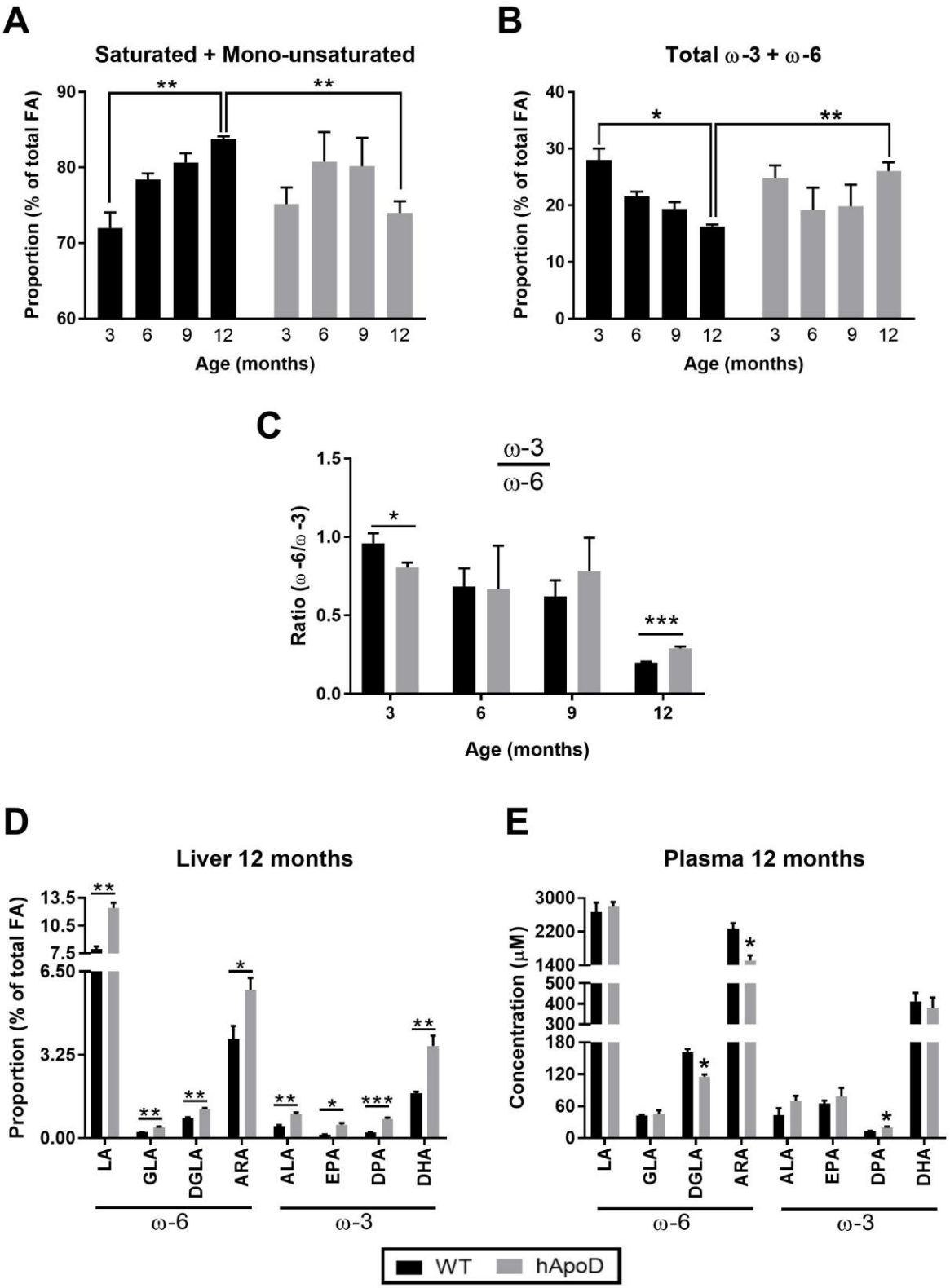
A
Saturated + Mono-unsaturated
Proportion (% of total FA)
Age (months)
B
Total ω-3 + ω-6
Proportion (% of total FA)
Age (months)
C
ω-3
ω-6
Ratio (ω-6/ω-3)
Age (months)
D
Liver 12 months
Proportion (% of total FA)
LA
GLA
DGLA
ARA
ALA
EPA
DPA
DHA
ω-6
ω-3
E
Plasma 12 months
Concentration (μM)
LA
GLA
DGLA
ARA
ALA
EPA
DPA
DHA
ω-6
ω-3
WT
hApoD

Figure 6

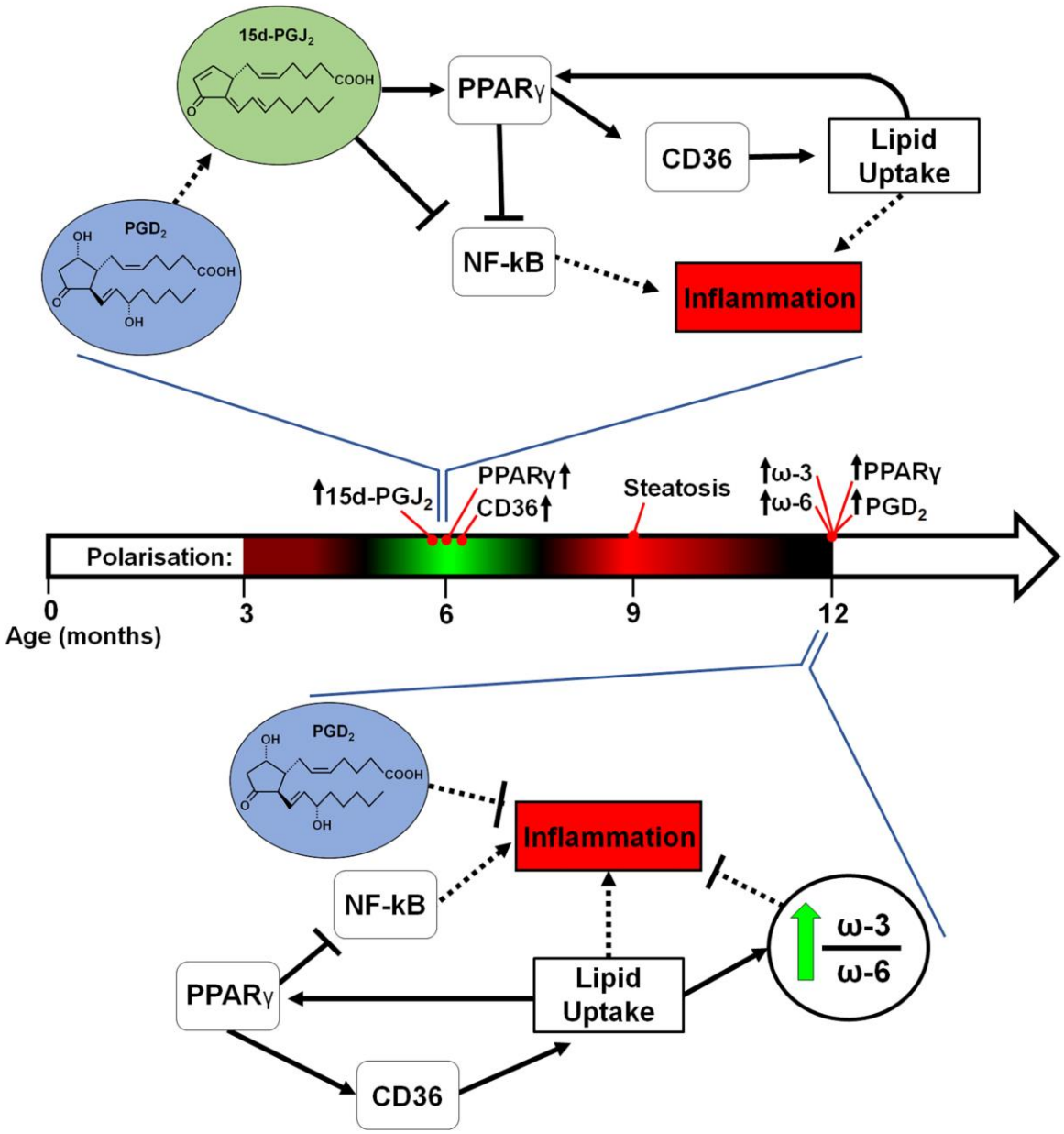
15d-PGJ2
COOH
PPARγ
CD36
Lipid Uptake
PGD2
OH
COOH
OH
NF-kB
Inflammation
↑15d-PGJ2
PPARγ↑
CD36↑
Steatosis
↑ω-3
↑ω-6
↑PPARγ
↑PGD2
Polarisation:
0
3
6
9
12
Age (months)
PGD2
OH
COOH
OH
Inflammation
NF-kB
ω-3
ω-6
PPARγ
Lipid Uptake
CD36

Figure 7

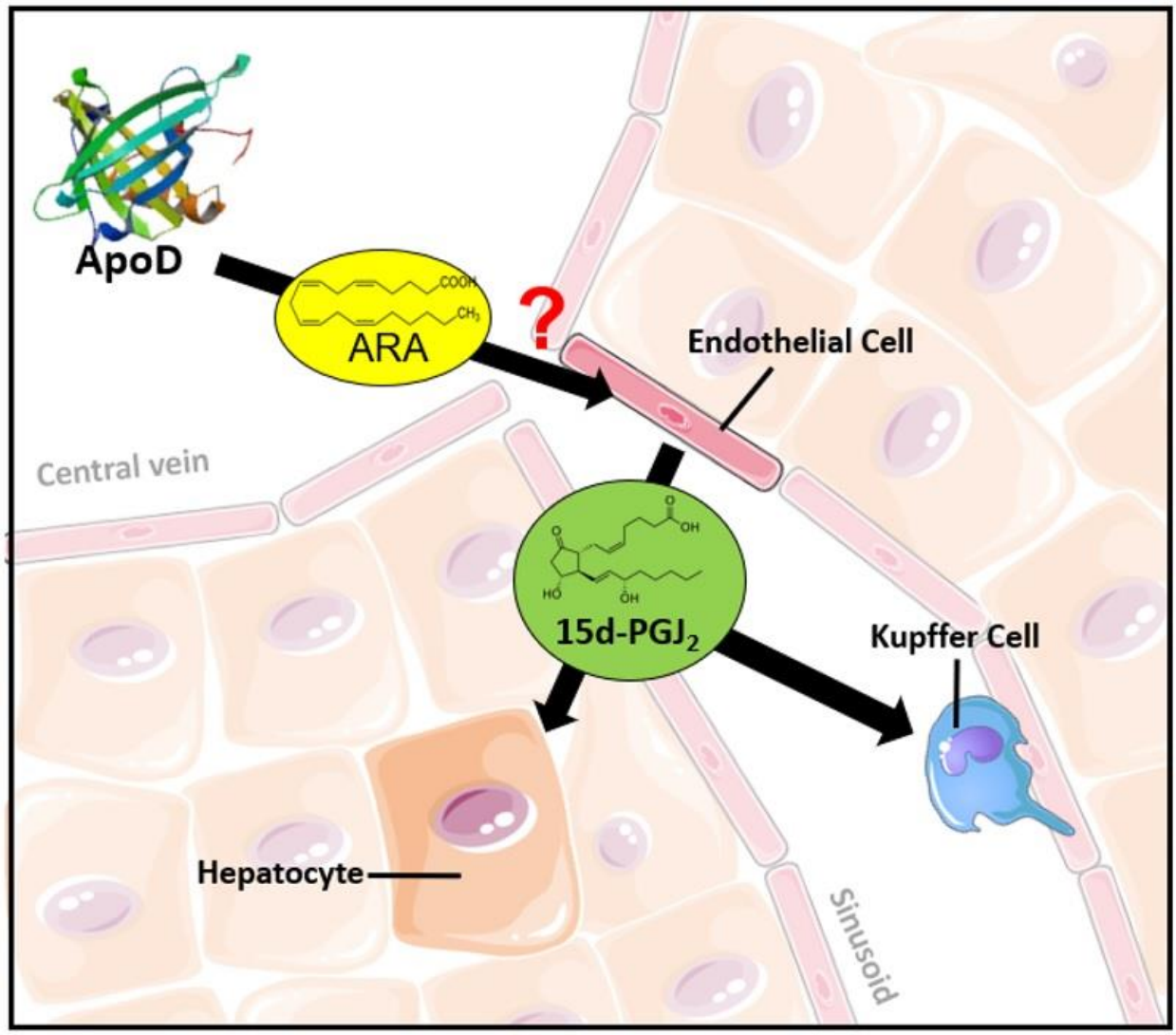
ApoD
ARA
COOH
CH3
?
Endothelial Cell
Central vein
15d-PGJ2
Kupffer Cell
Hepatocyte
Sinusoid

Figure Legends

Figure 1: ApoD overexpression increases hepatic lipid accumulation

Histological analysis of hepatic tissue from 3-, 6-, 9-, and 12-month-old wild type (WT) and transgenic hApoD mice (n=7-8 mice per genotype and per age). (**A**) Oil Red O staining with hematoxylin counterstain. Scale bar = 25 µm. *Right panel*: Quantification of Oil Red O staining. (**B**) Masson's trichrome staining. Arrows indicate macrovesicular steatosis. Scale bar = 25 µm. *Right panel*: Quantification of macrovesicular steatosis (Kleiner score modified for rodents) presented as box plots with overlaid data points. * *p<0.05, ** p<0.01* relative to WT controls.

Figure 2: Steatosis in hApoD mice is linked to PPARγ activation starting at 6 months

Protein and mRNA markers of lipogenesis (**A**, **B**) and lipid uptake (**C**, **D**) from 3-, 6-, 9-, and 12-month-old wild type (WT) and transgenic hApoD mouse livers (n=7-8 mice per genotype and per age). SREBP-1 activation in **A** is evaluated by determining the mature form/total protein ratio. Representative Western blots are provided for each protein target: SREBP-1 precursor form (~120 kDa), SREBP-1 mature form (~68 kDa), Amidoblack loading control, FASN and PPARγ. * *p<0.05, ** p<0.01* relative to WT controls.

Figure 3: Hepatic inflammatory polarization in hApoD mice

Evaluation of inflammation markers in 3-, 6-, 9-, and 12-month-old wild type (WT) and transgenic hApoD mouse livers (n=7-8 mice per genotype and per age). (**A**) Variation in macrophage polarization (M0 and M1, or M2) assessed via hepatic mRNA levels from hApoD mice relative to WT mice of the same age. Green indicates anti-inflammation polarization. Red indicates pro-inflammation polarization. When relevant, the *p*-value is provided. *Bottom panel*: Polarization index combining the contribution of all inflammation markers probed. (**B**) Quantification of macrophage recruitment foci in Masson's trichrome-stained liver slices (Kleiner score modified for rodents). *Inset panel*: Representative picture of inflammatory foci (highlighted in green). Scale bar = 25 µm. (**C**) Nuclear recruitment of NF-κB (p-50) assessed via western blotting of nuclear enriched liver fractions. Representative Western blots are provided for each time points. * *p<0.05, ** p<0.01*, *** *p<0.001* relative to WT controls.

Figure 4: Hepatic production of anti-inflammatory 15d-PGJ_2 in 6-month-old hApoD mice

Evaluation of prostaglandin production in 3-, 6-, 9-, and 12-month-old wild type (WT) and transgenic hApoD mouse livers (n=7-8 mice per genotype and per age). (**A**) Expression of key enzymes in prostanoïd synthesis. (**B**) Levels of prostaglandins PGE_2, PGD_2 and 15d-PGJ_2. *

p<0.05 relative to WT controls.

Figure 5: ApoD overexpression modulates omega acid hepatic content at 12 months

Evaluation of fatty acid proportions in 3-, 6-, 9-, and 12-month-old wild type (WT) and transgenic hApoD mice (n=3 mice per genotype and per age). (**A**) Proportion of hepatic [saturated + mono-unsaturated] fatty acids relative to total fatty acids. (**B**) Proportion of hepatic [ω-3 + ω-6] fatty acids relative to total. (**C**) Ratio of hepatic ω-3 *versus* ω-6 fatty acids. (**D**) Proportion of hepatic ω-3 and ω-6 fatty acids relative to total fatty acids at 12 months. (**E**) Plasma concentration of ω-3 and ω-6 fatty acids at 12 months. Fatty acids (FA) measured included: linoleic acid (LA), γ-linoleic acid (GLA), dihomo-γ-linoleic acid (DGLA), arachidonic acid (ARA), α-linolenic acid (ALA), eicosapentaenoic acid (EPA), docosapentaenoic acid (DPA) and docosahexaenoic acid (DHA). * *p<0.05, ** p<0.01, *** p<0.001*.

Figure 6: Model of inflammation control during the development of hepatic steatosis in hApoD mice

The overproduction of 15d-PGJ_2 at 6 months could activate the PPARγ transcription factor and trigger CD36 expression. CD36 mediates hepatic lipid uptake, which could create a feedback loop maintaining PPARγ activation after 6 months. Inflammation could be suppressed by 15d-PGJ_2-mediated inhibition of the IKK/NF-kB pathway. The overproduction of PGD_2 and preferential accumulation of ω-3 fatty acids by 12 months of age could also contribute to inflammation control. Hepatic macrophage polarization is represented along the timeline arrow: green indicates anti-inflammation polarization and red indicates pro-inflammation polarization. Blue lines indicate anti-inflammatory mechanism at relevant trimesters.

Figure 7: Cellular model for hepatic production of 15d-PGJ_2 in response to ApoD overexpression

Considering ApoD's capacity to bind ARA, it is highly plausible that its overexpression increases ARA transport to the liver. ARA import within hepatic endothelial cells could result in 15d-PGJ_2 production and diffusion, activating lipid uptake in hepatocytes as well as promoting M2 anti-inflammatory polarization in Kupffer cells and/or invading monocytes/macrophages.

SUPPLEMENTARY MATERIAL

Supplementary Table A1: Sequences of primers used in qPCR

Table A1: qPCR Primers Sequence

Gene	Forward (5'-3')	Reverse (5'-3')
HPRT1	TCA GTC AAC GGG GGA CAT AAA	GGG GCT GTA CTG CTT AAC CAG
CD36	AGA TGA CGT GGC AAA GAA CAG	CCT TGG CTA GAT AAC GAA CTC TG
FASN	GGC TCT ATG GAT TAC CCA AGC	CCA GTG TTC GTT CCT CGG A
CD68	CCC TGT GTG TCT GAT CTT GCT	ACA TTT CCG TGA CTG GTG GT
F4/80	GGA AAG CAC CAT GTT AGC TGC	CCT CTG GCT GCC AAG TTA ATG
IL-1β	GAA ATG CCA CCT TTT GAC AGT G	TGG ATG CTC TCA TCA GGA CAG
IL-6	CTG CAA GAG ACT TCC ATC CAG	AGT GGT ATA GAC AGG TCT GTT GG
TNF-α	CCC TCA CAC TCA GAT CAT CTT CT	GCT ACG ACG TGG GCT ACA G
TGF-β	CTT CAA TAC GTC AGA CAT TCG GG	GTA ACG CCA GGA ATT GTT GCT A
CD163	TGG GTG GGG AAA GCA TAA CT	AAG TTG TCG TCA CAC ACC GT
PTGS1	ATG AGT CGA AGG AGT CTC TCG	GCA CGG ATA GTA ACA ACA GGG A
PTGS2	TGA GCA ACT ATT CCA AAC CAG C	GCA CGT AGT CCT CGA TCA CTA TC
HPGDS	GTG AAC GGC AAA GTG GCT CT	TCC AAT CCA CCA ATG CTA CCT
PTGDS	TGC AGC CCA ACT TTC AAC AAG	ATA CAG CTT TCT TCT CCC GG

Supplementary Figure 1

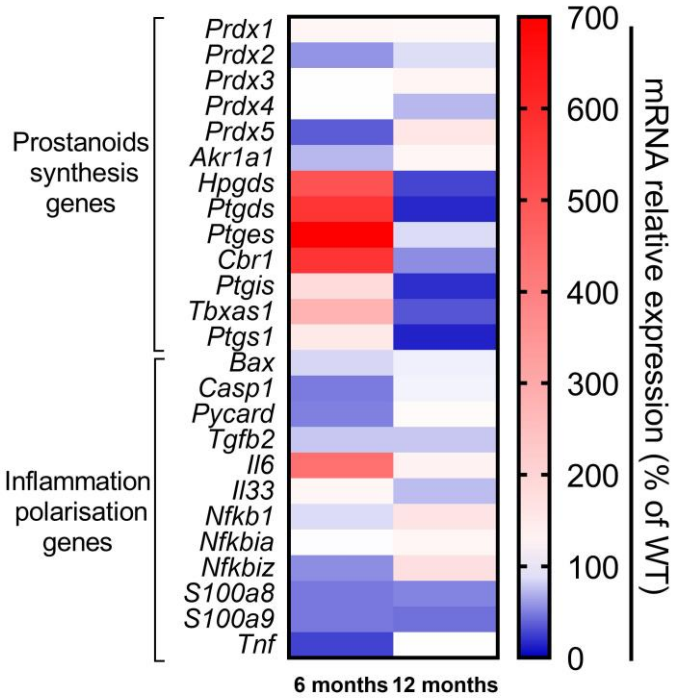

Supplementary Figure 2

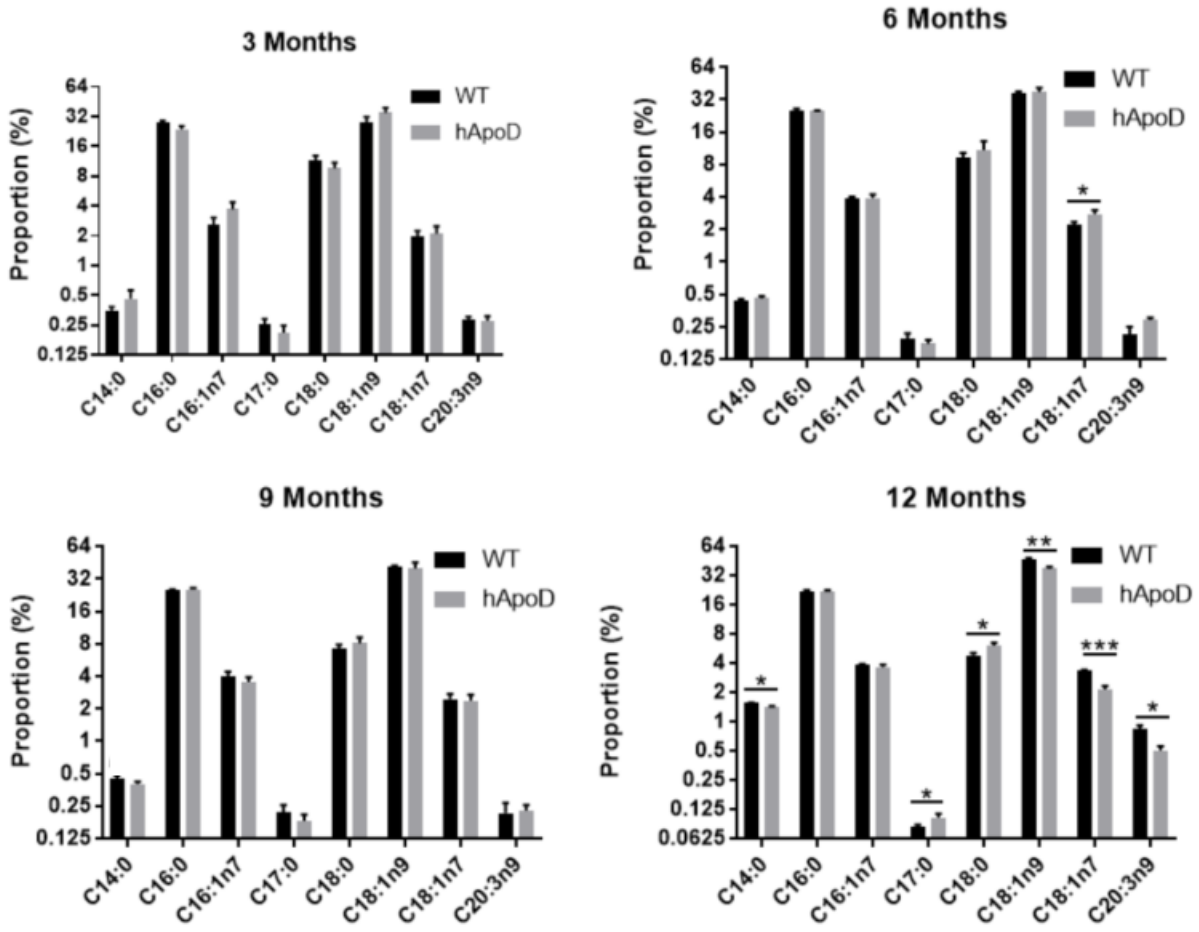

Supplementary Figure 3

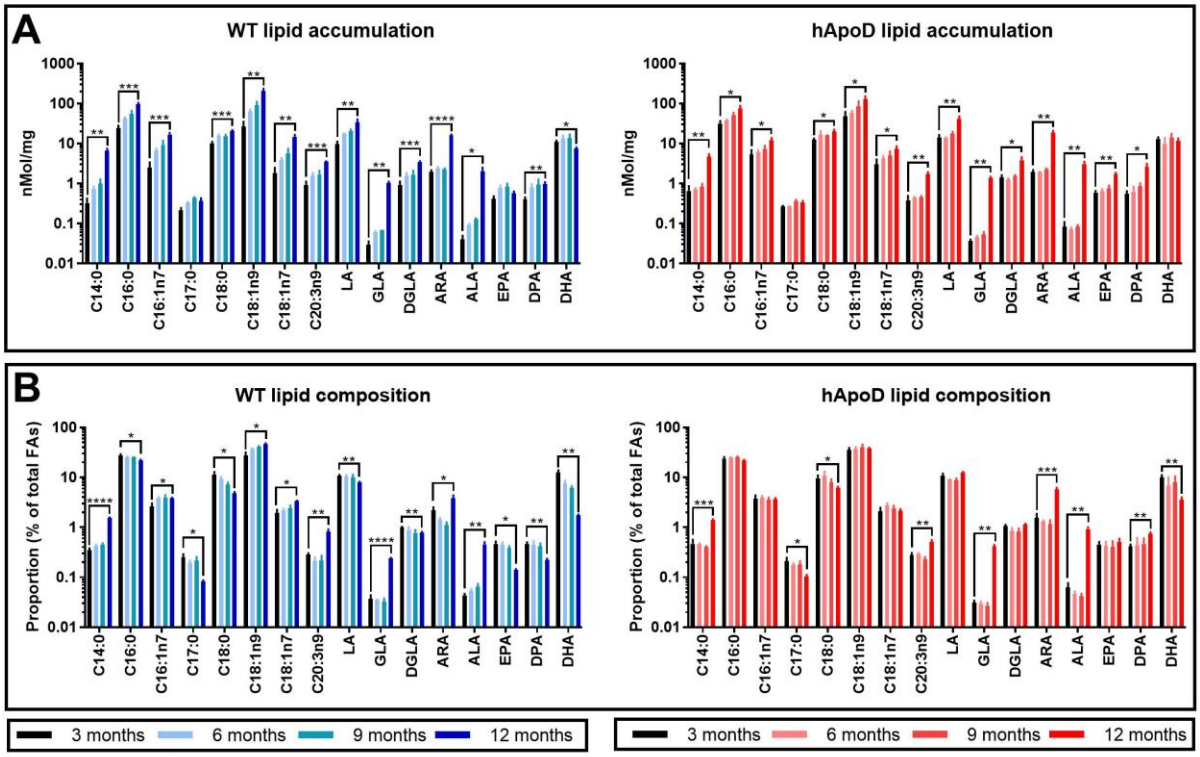

Supplementary Figure Legends

Supplementary Figure A1: Preliminary qPCR array panel

Preliminary screening of hepatic mRNA gene expression in 3- and 12-month-old hApoD mice compared to wild type (WT) control (n=1-2 mice per age). The panel includes important genes regulating inflammatory balance and prostaglandin synthesis.

Supplementary Figure A2: Additional lipids included in the GC-MS panel

Evaluation of hepatic fatty acid proportions relative to total fatty acids in 3-, 6-, 9-, and 12-month-old wild type (WT) and transgenic hApoD mice (n=3 mice per genotype and per age). Predominant hepatic saturated, mono-unsaturated and ω-9 fatty acids were measured (**A-D**). Fatty acids measured included: myristic acid (C14:0), palmitic acid (C16:0), palmitoleic acid (C16:1n7), margaric acid (C17:0), stearic acid (C18:0), oleic acid (C18:1n9), vaccenic acid (C18:1n7), nonadecanoic acid (19:0) and mead acid (C20:3n9). * *$p<0.05$, ** $p<0.01$, *** $p<0.001$*

Supplementary Figure A3: Effect of age on hepatic lipid accumulation and composition

Evaluation of fatty acid (**A**) concentration and (**B**) proportions relative to total fatty acids in 3-, 6-, 9-, and 12-month-old wild type (WT) and transgenic hApoD mice (n=3 mice per genotype and per age). Fatty acids (FA) measured included: myristic acid (C14:0), palmitic acid (C16:0), palmitoleic acid (C16:1n7), margaric acid (C17:0), stearic acid (C18:0), oleic acid (C18:1n9), vaccenic acid (C18:1n7), nonadecanoic acid (19:0), mead acid (C20:3n9), linoleic acid (LA), γ-linoleic acid (GLA), dihomo-γ-linoleic acid (DGLA), arachidonic acid (ARA), α-linolenic acid (ALA), eicosapentaenoic acid (EPA), docosapentaenoic acid (DPA) and docosahexaenoic acid (DHA). * *$p<0.05$, ** $p<0.01$, *** $p<0.001$*